(INVITED PAPER)

SUBMITTED JOURNAL OF SELECTED TOPICS IN QUANTUM ELECTRONICS

21/5/97

Wavelength-Swept Fiber Laser with Frequency Shifted Feedback and Resonantly Swept Intra-cavity Acousto-Optic Tunable Filter

S. H. Yun, D. J. Richardson, D. O. Culverhouse, B. Y. Kim

14-59

S. H. Yun and B. Y. Kim are with the Department of Physics, Korea Advanced Institute of Science and Technology (KAIST), 373-1 Kusong-dong, Yusong-gu, Taejon 305-701, KOREA

Tel :+82-42-869-2527, Fax:+82-42-869-5527, e-mail: yoonkim@sorak.kaist.ac.kr

D. J. Richardson and D. O. Culverhouse are with the Optoelectronics Research Center, University of Southampton, Southampton, SO17 1BJ, U.K.

ABSTRACT

This paper concerns a Wavelength-Swept Fiber Laser (WSFL) incorporating frequency shifted feedback and an intra-cavity passband filter, in which the wavelength of the modeless output is linearly, continuously and repeatedly tuned (in time) over a given range by modulation of the filter peak wavelength and filter strength. We show both numerically and experimentally that amplifier noise plays a key role in determining the operating modes of frequency-shifted fiber laser systems and that a 'noisy' amplifier can be used to suppress the natural tendency of such lasers to pulse allowing for continuous wave, modeless operation. Furthermore, we show that significant narrowing of a WSFL instantaneous swept linewidth can be obtained if the filter peak transmission wavelength is resonantly swept so as to follow the wavelength shift per pass due to the acousto-optic frequency shift. Using these ideas we go on to demonstrate and characterize a high power, diode-driven, Er^{3+}/Yb^{3+} WSFL incorporating a bulk-optic Acousto-Optic Tunable Filter (AOTF). Linewidths as narrow as 9 GHz, sweep ranges up to 38 nm and output powers as high as 100 mW are obtained. Furthermore, we demonstrate the generation of user definable average spectral output by synchronous modulation of the filter strength and multi-wavelength pulsed output at higher sweep rates. Excellent agreement between the experimental results and those of the numerical modelling is obtained. Our simulations show that reduced linewidth (<0.02 nm) and improved scan linearity should be readily achievable with realistic system improvements. We believe such sources to be of considerable physical and practical interest with applications ranging from sensor array monitoring, device characterization through to low coherence measurement technology.

I. INTRODUCTION

The combined effects of frequency-shifted feedback and optical filtering within a laser cavity can lead to a number of interesting regimes of laser operation and has attracted considerable attention within recent years. Most work in the area to date has considered the cavities in which light experiences a fixed frequency shift per round-trip and is filtered by a bandpass filter of fixed transmission, bandwidth and central frequency. In this instance, depending on the precise system characteristics, either high spectral brightness modeless laser output [1]-[5], or pulsed operation can be achieved [5]-[8]. In the mode-less laser case, the frequency shift per round-trip prevents a coherent build up of the laser mode-structure resulting in a broadband, mode-less output with a spectral envelope determined by the filter characteristic and the magnitude of the frequency shift. During pulsed operation trains of short (typically 10 ps - 1 ns) pulses are generated. The pulsed operation is self starting, and, unlike active mode-locking, does not require any resonant matching of the frequency shift per round-trip to the cavity round-trip frequency.

The tendency for pulsing is particularly strong in Frequency-Shifted Fiber Lasers (FSFL's) where stable trains of mode-locked pulses are typically generated. Recent work by Sabert et al. [6] has attributed the pulsing to the nonlinear Kerr effect occurring within the optical fiber. The FSFL intrinsically favors pulsed rather than continuous wave (cw) operation because a nonlinear pulse, restoring its spectrum by self phase modulation (SPM) after being shifted away from the filter peak wavelength by the frequency shifter, experiences less loss in the filter than linear radiation. Another way of viewing the pulse formation process is that the SPM of the intra-cavity field acts as a phase seeding mechanism, establishing a phase distribution

throughout the spectrum and eventually the formation of stable optical pulses. Such pulsed laser operation has much in common with the use of sliding-frequency filters for soliton control within soliton communications systems [9]. In this instance the central frequencies of noise reduction filters within a transmission line is slid such that soliton pulses, which can adjust their central frequencies to pass though the filtered line through the combined influence of nonlinearity and dispersion, suffer lower loss than linear radiation allowing for enhanced soliton transmission. Techniques for suppressing this pulsing in FSFL's are a key issue if one is interested in operating them in a mode-less laser mode.

With recent developments of Acousto-Optic Tunable Filters (AOTF's) it has become possible to envisage fiber laser cavities in which the filtering and frequency shift per round-trip are no longer fixed quantities but become time dependent. In particular, the possibility to rapidly and smoothly change the central frequency of a filter transmission peak by electronic means should allow for rapid, continuous sweeping of the output wavelength of a fiber laser [10]-[11]. Such Wavelength-Swept Fiber Lasers (WSFL's) have a wide number of applications ranging from low coherence interferometry [10], sensor interrogation, device instrumentation and characterization through to techniques such as Optical Frequency-Domain Reflectometry (OFDR) [12]-[14]. In particular, WSFL's offer an attractive option for simple and effective spectral demultiplexing schemes in fiber grating sensors, promising higher spectral density and narrower spectral resolution than the conventional methods utilizing a combination of broadband sources and scanning narrowband receivers [15]-[16].

The principal factor determining the operation of an WSFL relates to the interplay of the frequency shift (wavelength shift) and change in filter peak position per round-trip. Consider a WSFL having a filter and a frequency shifter in the cavity. On each round-trip, the laser spectrum in the cavity is shifted in frequency by f_{FS} and reshaped by a filter with a peak frequency shifted by f_{filter} in one round-trip time. In a spectral reference frame moving with the filter passband, the filter peak frequency is static, but the laser spectrum is shifted by $f_{FS} - f_{filter}$. The output characteristics of the WSFL are therefore largely predictable from those of a conventional FSFL laser with an unswept filter and an effective frequency shift $f_{FS} - f_{filter}$ per round-trip.

A simple model which ignores the influence of nonlinearity was developed by Streifer et. al. and Littler et. al. to predict the spectral characteristics of FSFL's and found to give reasonably good agreement with experiment [17]-[18]. The authors showed that the envelope of the FS laser output spectrum at a given optical power is determined only by the filter bandwidth, the frequency shift, and the spectral density of the spontaneously emitted light in the gain medium. The model also showed that the steady-state spectrum has its peak offset from the filter peak frequency. The offset frequency and the linewidth were proportional to, approximately, $b^{2/3} f_{FS}{}^{1/3}$ and $b^{2/3} |f_{FS}|^{1/3}$, respectively, where b is the filter bandwidth. This, on its own, implies both the offset and linewidth are minimized in the WSFL by matching the filter sweep rate to the frequency shift, *i.e.* $f_{filter} = f_{FS}$. This is illustrated in Fig. 1. In this resonant case, Amplified Spontaneous Emission (ASE) light generated under the filter peak at the start of the filter sweep remains under the peak as the filter is swept across the amplifier gain profile and consequently experiences significant spectral narrowing with respect to the non resonant case. From a

nonlinear perspective one might also hope that this would lead to a reduction in the tendency of the WSFL to pulse since, in the resonant case, it should be narrowband linear radiation moving under the peak center rather than a nonlinear pulse that should experience the least loss. In terms of our previous FSFL analogy with controlled soliton transmission systems the resonantly swept WSFL corresponds to a soliton transmission line with fixed filters with the same central frequency. Soliton transmission through such systems has been shown to be ultimately limited by preferential noise build up under the filter peak [9].

Recently we have implemented the above principles and demonstrated a wavelength-swept Er^{3+}/Yb^{3+} co-doped fiber laser incorporating an AOTF in the cavity; a cw modeless output, a sweep range as wide as 38 nm, a fast scan rate of some hundreds Hz, and a high output power of up to 100 mW have been achieved [11]. Our experimental results have indeed shown that the resonant matching of the filter peak sweep rate to the AO frequency shift leads to a significant narrowing of the instantaneous swept linewidth; a spectral resolution of <0.1 nm has been demonstrated. In this paper we investigate more fully the interplay between the AO induced frequency shift and change in filter central frequency per round-trip in a WSFL both experimentally and theoretically. We present the results of numerical modeling of the system that are in good agreement with our experimental observations. We also examine the role of amplifier noise on the operation of the system and show that resonant sweeping and a large amplifier noise figure can frustrate the pulse formation process inherent in FSFL systems.

II. EXPERIMENTAL AND SIMULATION DETAILS

A. Experimental Configuration

The WSFL configuration is shown in Fig. 2. The laser was in a unidirectional ring configuration and comprised a gain section, an output coupler and an AOTF. The AOTF was a bulk-optic device based on polarization conversion. The AO frequency shift associated with the filtering was around +68 MHz and the filter had a 4 nm bandwidth around 1550 nm. The transmission peak wavelength was tuned around 1550 nm by variation of the acoustic frequency with a slope coefficient of −20.6 nm/MHz. The total insertion loss of the AOTF was 2.5 dB for 0.7-W applied rf power. The amplitude and frequency of the acoustic drive to the AOTF were controlled by a phase lock loop (PLL) control circuit driven by two independent, but phase-locked, arbitrary waveform generators. The acoustic power to the AOTF was linearly dependent on the output voltage from one of the generators and the frequency linearly dependent on the output from the other. We could therefore synchronously and independently control the peak transmission and wavelength of the filter as a function of time.

Two fiber amplifier systems were available for use within the laser, each of which comprising an active fiber, two isolators, a WDM coupler, and a pump laser [Fig. 2(a)]. The first amplifier was based upon a 10-m-long Er^{3+}/Yb^{3+} co-doped fiber, backward pumped by a diode-driven Nd-YLF laser giving 600-mW maximum fiber-coupled output power at 1047 nm. The amplifier was considerably overlength from conventional amplifier design perspectives resulting in a large noise figure which was measured to be 20 dB (at 1555 nm) under operating conditions similar to those experienced within the cavity. The saturated output power from the amplifier system was 22 dBm and maximum small signal gain 22 dB (at 1550 nm). This amplifier was used in most of the experiments reported in this paper. The second amplifier was a low-noise, EDFA pumped in a co-propagating geometry with a 100 mW, 980 nm diode laser.

The small signal gain of the amplifier was 38 dB at the 1532 nm gain peak, and the saturated output power was 13 dBm. The amplifier noise figure was measured to be 5 dB at the gain peak.

Light was extracted from the cavity by a 90% output coupler (unless otherwise stated). The total cavity length was around 20 m (for both amplifier options). Control of the intra-cavity birefringence was provided through incorporation of two polarization controllers in the cavity (before and after the AOTF). The cavity round-trip loss excluding output coupling was approximately 3 dB.

B. Numerical model

In order to understand the detailed behavior of our laser and to enable us to identify the key system parameters we developed a numerical model with which to simulate our system. The parameters used for most of the modeling presented here were based on our experimental values. The gain, loss, nonlinear Kerr-effect, dispersion, frequency shift, and spectral filtering were treated as lumped [Fig. 2(b)]. We defined intra-cavity complex field amplitudes, on a m-th round-trip, $e_m(t)$ ($\sqrt{\mathrm{W}}$) in the time domain and $a_m(\nu)$ ($\sqrt{\mathrm{J/Hz}}$) in the spectral domain. Their squares are respectively the temporal and spectral power densities at the output end of the amplifier. The average output power $\dot{P}_{out}$ extracted by the 90% port of the output coupler is given by

$$P_{out} = \frac{\Gamma_1}{\tau_{rt}} \int_{-\infty}^{\infty} |e_m(t)|^2 \, dt = \frac{\Gamma_1}{\tau_{rt}} \int_{-\infty}^{\infty} |a_m(\nu)|^2 \, d\nu , \qquad (1)$$

where $\Gamma_1 = 0.45$ represents the optical power attenuation arising between the output ports of the amplifier and the coupler, and $\tau_{rt} = 100$ ns is the round-trip time. It can be shown that $a_m(\nu)$ and $e_m(t)$ are related to each other by the Fourier Transform:

$$a_m(\nu) = \int_{-\infty}^{\infty} e_m(t)\, e^{i2\pi\nu t}\, dt, \text{ and } e_m(t) = \int_{-\infty}^{\infty} a_m(\nu) e^{-i2\pi\nu t}\, d\nu. \quad (2)$$

Physically, $e_m(t)$ is related to the real-valued electric field amplitude $E(z=0, t) = \sqrt{2Z/(\pi r^2)}\, Re\{e(t)\}$, where $Z = 258\ \Omega$ is the impedance of the optical fiber, $r = 4\ \mu$m the mode-field radius of the fiber, and $e_m(t) = e(t)$ if $m \cdot \tau_{rt} < t \le (m+1) \cdot \tau_{rt}$ and $e_m(t) = 0$ elsewhere.

Evolution of the laser spectrum on successive round-trip is governed by the following equation [6]:

$$a_{m+1}(\nu + f_{FS}) = \sqrt{G_m \Gamma_{tot} T_m(\nu)}\, e^{i\beta(\nu)L} \{a_m(\nu) + a_m^{ASE}(\nu) + a_m^{nl}(\nu)\}. \quad (3)$$

Here, $\Gamma_{tot} = 0.05$ represents the total cavity loss (13 dB), and

$$G_m = \exp\left[\frac{\ln G_0}{1 + \eta \cdot P_{in}}\right] \quad (4)$$

is the saturated amplifier gain. Here G_0 is the small-signal gain, $P_{in} = \frac{\Gamma_{tot}}{\tau_{rt}} \int_{-\infty}^{\infty} |a_m(\nu)|^2\, d\nu$ is the input optical power to the amplifier, and the multiplication factor $\eta = 0.0528$ is determined from the the saturation input power of 3 mW at the maximum small signal gain of 22 dB. $T_m(\nu) = \exp[-4\ln 2\ (\nu-\nu_m)^2/b^2]$ is a Gaussian filter transmission function where ν_m is the center frequency of the filter passband ($\nu_{m+1} - \nu_m = f_{filter}$), and b = 500 GHz (4 nm) is the FWHM bandwidth of the filter. $\beta(\nu)$ is the propagation constant expanded up to the second-order

dispersion term $\beta_2(\nu-\nu_m)^2$ where $\beta_2 = 1/(2\pi)^2 d^2\beta/d\nu^2 = -20$ ps^2/km. $L = 20$ m is the total cavity length. The second term in the curly bracket of Eq. (3) represents the addition of noise spectrum due to ASE of the gain medium [19]:

$$a_m^{ASE}(\nu) = \sqrt{0.5 \cdot (1/\Gamma_{tot}) \cdot NF \cdot h\nu_0 \cdot \tau_{rt}}\, e^{i\varphi_m(\nu)}. \quad (5)$$

Here $NF = 100$ is the noise figure of the amplifier, $h\nu_0 = 1.27\ 10^{-19}$ J is the single photon energy at $\lambda = 1558$ nm, $\varphi_m(\nu)$ is the random phase function ranging between 0 and 2π, and the multiplication factor 0.5 comes from the fact that only one polarization state contributes to the laser build up. The last term of Eq. (3) describes the nonlinear Kerr effect: $a_m^{nl}(\nu) = \int_{-\infty}^{\infty} e_m(t)\,(e^{i\phi_m^{nl}(t)} - 1)\, e^{i2\pi\nu t}\, dt$. Here, $\phi_m^{nl}(t) = (2\pi/\lambda)\, n_2\, L_{nl}\, I_m(t)$ where $n_2 = 3.2\ 10^{-20}$ m^2/W is the nonlinear refractive index, $L_{nl} = 10$ m is the effective length of a nonlinear interaction medium, and $I_m(t) = |e_m(t)|^2/(\pi r^2)$ is the effective optical intensity in the nonlinear medium. We assumed the laser build up to start from the initial ASE noise, i.e. $a_{m=0}(\nu) = a_{m=0}^{ASE}(\nu)$.

The model is encoded in a PC for numerical simulation [Appendix]. We defined a window in the spectral domain, which was represented by 2048 discrete frequency components with an equal spacing of $\Delta = 100$ MHz. The total window thus spanned 204.8 GHz. For convenience in computer coding, the center frequency of the window was made to shift by f_{FS} per round-trip. Using this moving reference frame, we were able to choose the value of Δ without restriction that, otherwise, the spacing Δ should be equal to or a sub-harmonic of f_{FS} to simulate the frequency shift properly without passing on any phase information between

the frequency components. In this frame, the filter passband is seen to move by $f_{filter} - f_{FS}$ per round-trip. As the filter passband is swept, the laser spectrum is shifted and would eventually escape the spectral window unless the position of the window is re-adjusted to contain the laser spectrum. To avoid this problem, we shifted the window in the spectral domain occasionally once the filter peak frequency deviated significantly from the center of the window so that the filter peak frequency returns to near the window center avoiding edge effects at the frequency grid edges. The frequency shift f_{FS} was assumed to be a constant of +68 MHz although the actual experimental value was varied over a small range in time so as to sweep the filter wavelength with a tuning coefficient of about −50 kHz/nm.

III. Experimental and Numerical Results

A. Laser operating mode under unswept filter characteristics

We first examined FSFL operation with fixed AOTF characteristics. Initially, we numerically investigated how the mode of operation (pulsed or cw) depended on the various system parameters. We started off by neglecting the effects of amplifier noise and concerned ourselves with the filtering, frequency shifting and propagation effects alone. Our conclusion was that nonlinearity plays the key role in the pulse formation process in agreement with the earlier findings of Sabert and Brinkmeyer [6]. Indeed we reproduced the results presented in their earlier work in validating this part of our code.

We next included the effects of amplifier noise in the simulation to see if this altered the situation and found that once a realistic amount of ASE noise light was added to the system pulse formation was hindered. The majority of simulation results related to the physical

parameters of the experimental system previously described containing the noisy Er^{3+}/Yb^{3+} amplifier with 20-dB noise figure. The resultant spectral power density of ASE noise $|a_m^{ASE}(\nu)|^2$ was calculated to be 1.273 10^{-23} J/Hz from Eq. (5). Fig. 3 shows the simulation results for the temporal and spectral power spectra taken after 3000 round-trips at the end of the amplifier. The output power was 10 mW. When the correct value for ASE power was used, the laser output were effectively cw, as shown in Fig. 3(a). When the ASE power was reduced by two orders of magnitude, a strong tendency of multiple pulse generation was observed, as shown in Fig. 3(c). These results therefore indicated that the addition of strong, randomly phased noise to the re-circulated, non-linearly generated seed signal can prevent the build up of a constant phase relationship across the emission spectral bandwidth, thereby frustrating the formation of pulsed output.

The validity of this idea was confirmed by the following experiments. We examined the system operation of the FSFL under fixed filter operation for intra-cavity amplifiers with both low and high noise gain characteristics. Initially we used the low-noise 980-nm pumped amplifier previously described. Output coupling from the laser in this instance was arranged to be from the 10% port of the output coupler. The laser was found to produce self-starting pulses for almost all settings of the intra-cavity polarization controllers at a few 10's of mW of launched pump power. Pulsed operation was by far the preferred mode of operation for this laser configuration. The pulsing was characteristic of that of most forms of passively mode-locked soliton fiber laser with chaotic pulsing at high average powers and stabilized pulse bunches at low pump power. Stable fundamental mode-locking was readily obtained by

accurate control of the pump power. Pulsing was also largely sustained during resonant sweeping of the filter central frequency.

The low noise amplifier was then replaced with the large noise-figure Er^{3+}/Yb^{3+} amplifier. In addition, we increased the total cavity loss by taking the output from the 90% port of the output coupler. The ASE noise power was consequently increased by two orders of magnitude relative to our previous experiment. In this instance the laser output was typically a continuous wave. Only near the threshold pump power and by very careful alignment of the fiber polarization controllers did we ever manage to observe any form of pulsing. Once the filter peak was swept any possibility for pulsed operation was completely lost. The modeless CW linewidth was between 30-50 GHz depending on the laser output power.

B. Instantaneous linewidth measurements

We next systematically examined the laser performance under swept operation for the cavity incorporating the Er^{3+}/Yb^{3-} amplifier and 90% output coupling. Initially we examined a linear sweep in filter peak wavelength. The linear wavelength sweep was accomplished by linearly chirping the applied acoustic frequency to the device. Practically this was achieved by applying a saw-tooth waveform to the frequency control input of the AOTF control system. The filter peak wavelength was thereby linearly swept between fixed wavelength extremes defined by the amplitude and DC offset of the saw-tooth wave at a sweep frequency f_{sweep}. As the acoustic frequency is swept upward in frequency, the filter central wavelength, and thereby the wavelength of the output radiation, is swept downward in wavelength. The resonant saw-tooth sweep frequency depended on the sweep range, cavity length and AO frequency shift per pass:

For example, in the case of a 20 nm (2.5 THz) sweep, f_{FS} = 68 MHz and a cavity round-trip frequency of 10 MHz, the resonant sweep frequency is calculated to be 275 Hz. It should be noted that resonant sweeping across the full frequency range should actually require a slightly nonlinear wavelength variation with time since the acoustic shift per pass varies slightly as the filter peak wavelength is swept. The 20 nm sweep requires a 1 MHz or ~1.5% variation in the magnitude of frequency shift. We designed exponential-type wavelength sweeps to correct for this higher order effect but no significant difference was observed from the simpler linear sweep for the experimental measurements made to date. The acoustic amplitude was kept constant across the full frequency sweep range for our initial experiments.

We started our experiments by examining the instantaneous linewidth of the swept laser output as a function of sweep frequency. The measurement was made at a fixed wavelength within the scan range by examining the temporal response of the reflection of the swept laser output from a fixed narrowband fiber grating (bandwidth 7 GHz, centered at 1558 nm) [Fig. 2(a)]. The reflected temporal pulse form is directly related to a correlation overlap between the laser output spectrum and the grating reflectivity profile. The temporal width ξ of the reflected pulse determines the instantaneous linewidth $\Delta\nu$ at the grating peak wavelength. Assuming that the output spectrum and the grating reflection profile both have Gaussian forms, we get

$$\Delta\nu = [(f_{filter}\,\xi/\tau_{rt})^2 - b_{grating}^2]^{1/2}, \tag{3}$$

where $b_{grating}$ = 7 GHz is the grating bandwidth. Moreover, by measuring the absolute arrival time of the return pulse and by comparing it with the calibrated position of the sliding filter peak we were able to ascertain the exact position of the center of the laser output spectrum relative to

the filter peak. We plot in Fig. 4 the typical temporal return from the fiber grating at three different sweep frequencies of 250, 270, and 290 Hz for an output power of 3 mW. The temporal width of the reflected signal has a minimum around f_{sweep} = 270 Hz. The reflected output deviates from a Gaussian either side of resonance (250 and 290 Hz). This is in agreement with the previous reports that the conventional unswept FSFL laser produce an asymmetric spectrum [1], [3], [6], [Fig. 1]. Assuming the offset frequency to be zero at f_{sweep} = 270 Hz, we mark the position of the filter peak frequency with a dotted line in Fig. 4 clearly illustrating that the pulse locates itself on opposite sides of the filter peak either side of resonance. On resonance the spectrum locates itself under the peak of the effective gain curve.

From this experiment, we could measure the instantaneous linewidth and offset from the filter center as a function of sweep frequency. Fig. 5 shows the measured linewidth for the 20-nm wavelength sweep from 1544 nm to 1564 nm at two different output power levels of 3 and 100 mW. It is seen that a significant reduction in instantaneous linewidth was indeed observed as anticipated at a frequency of around 270 Hz, close to that predicted for resonant sliding of the filter peak. However, it should be noted that the exact position of the resonant peak varied slightly (+/- 20Hz) depending on the states of the polarization controllers. We attribute this variation to the polarization dependence of the AOTF associated with the wavelength-dependent cavity birefringence. This effect locally affects the sliding rate of the overall gain shape and thereby effective resonant sweep rate. At low output powers of a few mW, the measured linewidths were ~30 GHz away from resonance, however these narrowed up to as low as 9 GHz (0.072 nm) on resonance. At high output power of around 100 mW, the minimum achievable linewidths were limited to 25 GHz or so, as opposed to the non-resonant linewidths of order

50-60 GHz. The measurements were repeated for wavelength sweeps ranging from 2 to 38 nm for both linear and exact exponential wavelength sweeps but no further linewidth reduction was possible.

Fig. 6 shows the measured offset frequency between the spectral peak of the laser output and the center frequency of the filter for the 20 nm sweep at 3 mW output power level. As expected, the spectrum locates itself at opposite sides of the filter peak for sweep frequencies greater and less than the resonant case.

We simulated the WSFL using the code described previously for a variety of filter sweep frequencies around resonance. The initial noise spectrum was found to stabilize after an initial transient stage and reach the final steady state envelope after a few hundred to a few thousand round-trips, depending on the filter sweep rate. The spectral offset and width were measured and averaged from m = 3000 to 4500 round-trips. The results for output powers of 3 and 100 mW are shown by dashed lines in Figures 5 and 6. For these plots small-signal gains of 13.25 dB (G_0 = 21.13) and 20.8 dB (G_0 = 120.2) were chosen for the 3 and 100 mW output powers, respectively, and the total cavity loss was 13 dB (L_{tot} = 0.05).

From Figures 5 and 6, it is seen that the numerical modeling is in excellent agreement with our experimental observation, except for some discrepancy for the case of 100-mW output power, predicting both the expected fall off in linewidth for resonant sweeping, the correct spectral linewidth both on and off resonance and the correct degree of linewidth broadening associated with the increased output power. Interestingly, we found from our simulations that without the

nonlinear effect, *i.e.* $n_2 = 0$, as the output power increased, the spectrum moved farther away from the filter center frequency, and the linewidth decreased because of the increasing slope of the filter transmission profile. However, the opposite occurred when the nonlinearity was turned on i.e. as the output power increased, the offset decreased, and the linewidth increased, due to the additional SPM.

Having validated our model against experimental data we went on to investigate the possibility for further linewidth reduction by reduction of the filter bandwidth. The expected linewidth as a function of filter sweep rate at sweep rates around resonance are shown in Fig. 7(a) for values of intra-cavity filter bandwidth of 0.1, 0.4, and 1 nm. Significant reductions in linewidth were obtained on resonance as with the 4 nm filter. A plot of the minimum (resonant) linewidth as a function of filter width is given in Fig. 7(b) where it is seen that considerable reductions in swept linewidth can be envisaged. For example, a 1-nm filter results in a swept bandwidth of 2.5 GHz (<0.02 nm).

C. Absolute wavelength accuracy

In order to experimentally determine the absolute wavelength accuracy of the source across the full wavelength span we sampled the output at fixed time delays from the start of the wavelength scan by using an acousto-optic switch. The switch was held open for 2 μs after a given delay time, and the peak wavelength of the output was measured on an optical spectrum analyzer of 0.05-nm resolution using the max-hold, or average measurement option. The experimental values from the resonant tracked case could then be compared with that predicted from the calibrated, linear filter tuning characteristic. The results are plotted in Fig. 8(a) where

we see that reasonably linear tuning characteristics are obtained over the full scan. The RMS deviation from the desired linear tuning curves was 0.153 nm with a peak-to-peak deviation of <0.4 nm over the 20 nm range [Fig. 8(b)]. The deviations are attributed to the wavelength-dependent gain profile of the amplifier and birefringence in the cavity and could in principle be eliminated by higher order corrections of the filter sweep characteristics.

D. Time average spectral output

The time average output from the source as measured on the peak hold function of the optical spectrum analyzer over repeated scans on resonance is shown in Fig. 9 where we see that a well defined square average output spectrum was obtained with less than 1.0 dB variation across the full sweep range of 20 nm (average output power 100 mW). Variations of <0.4 dB (output power 102 mW) and <6 dB (output power 91 mW) were achieved for resonant sweeps of 10 nm and the maximum 38 nm, respectively. A plot of typical time domain behavior under resonant sweeping conditions is shown in Fig. 10 where it is seen that after a brief period of relaxation oscillation at the beginning of the wavelength sweep the output settles to a reasonably level continuous wave output over the remainder of the scan.

The spectral shape and output power were almost independent of the sweep frequency up to 7 kHz at the maximum pump power. However, as the sweep frequency increased higher than 7 kHz, the relaxation oscillation at the beginning of the sweep became so significant that the pulsed outputs were obtained, as shown in Fig. 11 in the case of a 10 nm sweep at f_{sweep} = 9.3 kHz. The pulse repetition rate was ~80 kHz and output power 60 mW. Each individual pulse

had a duration of order 1 μs and was associated with one of the peaks in the spectral domain. The harder the system was pumped the greater the number of pulses per sweep cycle.

Finally we also investigated the possibilities for designer average spectral output profiles by simultaneously varying the strength of the acoustic drive as its frequency is tuned. For this purpose we demonstrate the generation of triangular and square wave modulated forms over a 10 nm wavelength span by the application of triangular and square wave drives to the AOTF amplitude control [Fig. 12].

IV. CONCLUSIONS

We have investigated both numerically and experimentally the performance and key factors governing the operation of both FSFL and WSFL. We numerically demonstrated that the interplay between nonlinearity and amplifier noise plays a key role in determining whether a FSFL system operates in a cw, or pulsed mode and have gone on to show that resonant tracking of the filter peak to the total AO frequency shift experienced by light circulating within the cavity of a WSFL gives a reduction in the instantaneous swept linewidth to <0.1 nm bandwidth.

Using these design concepts we have developed and characterized a diode-pumped, high-power (up to 100 mW), wavelength-swept Er^{3+}/Yb^{3+} co-doped fiber laser in which the output wavelength is continuously and repeatedly tuned over a broad range (up to 38 nm) by modulation of the intra-cavity AOTF peak wavelength with an instantaneous swept linewidth of <9 GHz. An absolute RMS wavelength stability of 0.15 nm has been obtained over a sweep range of 20 nm. In addition, we have demonstrated that simultaneous control of the AOTF

transmission can allow the generation of user definable average spectral output profiles and that novel multi-wavelength pulsed output can be generated at high filter sweep rates. Good quantitative agreement between experiment and theory has been obtained.

Our simulations have indicated that even narrower spectral linewidth and better absolute wavelength accuracy can be achieved by moving to an AOTF with reduced spectral bandwidth. For example a 1-nm tunable filter should give <0.02-nm swept linewidth with anticipated improvement in absolute wavelength accuracy. We believe such sources to be of considerable physical and practical interest with applications such as sensor array monitoring, device characterization, and low coherence measurement technology.

ACKNOWLEGMENT

S. H. Yun acknowledges the financial support of the British Council and the Korea Science and Engineering Foundation during his stay at the ORC, and DJR gratefully acknowledges the support of the Royal Society through the provision of a Royal University Fellowship.

APPENDIX

From Eq. (3), we obtain:

$$a_{m+1}[k] = \sqrt{G_m \Gamma_m T_m[k]} \exp[i\frac{\beta_2}{2} L(k-k_m)^2 \Delta^2] \{a_m[k] + a^{ASE} + a_m^{nl}[k]\}, \quad \text{(A.1)}$$

$$T_m[k] = \exp[-4\ln 2 \cdot (k-k_m)^2 / b^2], \quad \text{(A.2)}$$

$$k_{m+1} = k_m + (f_{filter} - f_{FS}) / \Delta. \quad \text{(A.3)}$$

$$a_m^{nl}[k] = FFT\{e_n[j] \cdot (e^{i\Phi_{nl}[j]} - 1)\}, \quad \text{(A.4)}$$

$$\phi_m[j] = (2\pi / \lambda) n_2 L \cdot I_m[j], \tag{A.5}$$

$$I_m[j] = |e_m[j]|^2 / (\pi r^2) \Delta^2 \cdot (1 / T\Delta) . \tag{A.6}$$

Here $a_m[k]$'s are 2048 frequency components and $e_m[j]$'s represent 2048 electric-field components in the time domain defined by the delayed time $\tau_m = t - z/c_m$ where $c_m = 2\pi (d\beta/dv)^{-1}$ is the group velocity of light at the filter peak frequency. These two arrays are related to each other by the discrete Fast Fourier Transform (FFT).

The factor $1/T\Delta$ on the right-hand side of Eq. (A,6) was introduced for the following reason. The size of the time window $1/\Delta$ = 10 ns is only one tenth of the cavity round-trip time T_{rt} = 100 ns. If a cw light is to be dealt with, the non-zero temporal amplitudes outside the time window are actually folded into the window, making $|e_m[j]|^2$ ten times larger than those values that would be obtained when $1/\Delta$ is equal to T_{rt}. We circumvented this problem by introducing the correction factor $1/(T\Delta)$. While this argument does not apply to the case of a pulsed output, the correction factor are needed for most of our simulations which produce effectively cw outputs.

References

[1] W. Streifer and J. R. Whinnery, "Analysis of a dye laser tuned by acousto-optic filter," Appl. Phys. Lett., vol. 17, pp. 335-337, 1970.

[2] F. V. Kowalski, P. D. Hale, and S. J. Shattil, "Broadband continuous-wave laser," Opt. Lett., vol. 13, pp. 622-624, 1988.

[3] I. C. Littler, S. Balle, and K. Bergmann, "Continuous-wave laser without frequency-domain-mode structure: Investigation of emission properties and buildup dynamics," J. Opt. Soc. Amer. B., vol. 8, pp. 1412-1420, 1991.

[4] P. F. Wysocki, M. J. K. Digonnet, and B. Y. Kim, "Electronically tunable, 1.55-μm erbium-doped fiber laser," Opt. Lett., vol. 15, pp. 273-275, 1990.

[5] S. H. Yun, I. K. Hwang, and B. Y. Kim, "All-fiber tunable filter and laser based on two mode fiber," Opt. Lett., vol. 21, pp. 27-29, 1996.

[6] H. Sabert and E. Brinkmeyer, "Pulse generation in fiber lasers with frequency shifted feedback," J. Lightwave Technol., vol. 12, pp. 1360-1368, 1994.

[7] F. Fontana, L. Bossalini, P. Franco, M. Midrio, M. Romagnoli, and S. Wabnitz, "Self-starting sliding-frequency fiber soliton laser," Electron. Lett., vol. 30, pp. 321-322, 1994.

[8] D. O. Culverhouse, D. J. Richardson, T. A. Birks, and P. St. J. Russell, "All-fiber sliding-frequency Er^{3+} / Yb^{3+} soliton laser," Opt. Lett., vol. 20, pp. 2381-2383, 1995.

[9] L. F. Mollenauer, J. P. Gordon, and S. J. Evangelides, "The sliding-frequency guiding filter: An improved form of soliton jitter control," Opt. Lett., vol. 17, pp. 1575-1577, 1992.

[10] P. F. Wysocki, M. J. F. Digonnet, and B. Y. Kim, "Broad-spectrum, wavelength-swept, erbium-doped fiber laser at 1.55 μm," Opt. Lett. vol. 15, pp. 879-881, 1990.

[11] S. H. Yun, D. J. Richardson, D. O. Culverhouse, and B. Y. Kim, "Wavelength-swept fiber laser with frequency-shifted feedback," in Proc. of OFC'97, vol. 6. (Dallas, USA, 1997), pp. 30-31.

[12] W. V. Sorin, D. K. Donald, S. A. Newton, and M. Nazarathy, "Coherent FMCW reflectometry using a temperature tuned Nd:YAG ring laser," IEEE Photon. Technol. Lett., vol. 2, pp. 902-904, 1990.

[13] U. Glombitza and E Brinkmeyer, "Coherent frequency-domain reflectometry for characterization of single-mode integrated-optical waveguides," J. Lightwave Technol., vol. 11, pp. 1377-1384, 1993.

[14] S. R. Chinn, E. A. Swanson, and J. G. Fujimoto, "Optical coherence tomography using a frequency-tunable optical source," Opt. Lett., vol. 22, pp. 340-342, 1997.

[15] M. A. Davis, D. G. Bellemore, M. A. Putnam, and A. D. Kersey, "A 60 element fiber Bragg grating sensor system," in Proc. of OFS-11 (Sapporo, Japan, 1996), pp. 100-103.

[16] M. G. Xu, H. Geiger, and J. P. Dakin, "Modeling and performance analysis of a fiber Bragg grating interrogation system using an acousto-optic tunable filter," J. of Lightwave Technol., vol. 14, pp. 391-396, 1996.

[17] W. Streifer and P. Saltz, "Transient analysis of an electronically tunable dye laser-part II: analytic study," IEEE J. Quantum Electron., vol. QE-9, pp. 563- 569, 1973.

[18] I. C. M. Littler and J. H. Eschner, "The cw modeless laser: model calculations of an active frequency shifted feedback cavity," Opt. Commun., vol. 87, pp. 44-52, 1992.

[19] E. Desurvire, *Erbium-doped fiber amplifiers: principles and applications*. New York, USA: John Wiley & Sons, 1994, ch. 2.

Figure Captions

Fig. 1. Schematic of the laser spectrum in a wavelength swept laser when (a) $f_{filter} > f_{FS}$, (b) $f_{filter} < f_{FS}$, and (c) $f_{filter} = f_{FS}$.

Fig. 2. (a) Experimental fiber laser with a spectral analysis setup. (b) Schematic diagram of the laser used in the computer simulation.

Fig. 3. Simulation results for the spectral and temporal power densities at an laser output power of 10 mW. Temporal results: (a) and (c), spectral results: (b) and (d). The ASE spectral power densities used were $1.723\ 10^{-23}$ J/Hz for (a) and (b), and $1.723\ 10^{-25}$ J/Hz for (c) and (d), respectively.

Fig. 4. The laser output on reflection from a narrowband fiber grating at a sweep frequency of (a) 250 Hz, (b) 270 Hz (close to the resonant sweep), and (c) 290 Hz. Its temporal width is related to the laser linewidth. The dotted lines indicate the filter peak wavelengths. The anticipated spectral asymmetry is evident in (a) and (c) [Fig. 1].

Fig. 5 Linewidths at (a) 3-mW and (b) 100-mW output power levels as a function of sweep frequency for the 20 nm total wavelength sweep (data points: experimental values, dashed lines: numerical simulations).

Fig. 6. Offset frequencies at (a) 3-mW and (b) 100-mW output power levels as a function of sweep frequency for the 20 nm total wavelength sweep (data points: experimental values, dashed lines: numerical simulations).

Fig. 7. Simulation results: (a) Laser linewidth vs Filter sweep frequency at filter bandwidths of 1 nm (solid square), 0.4 nm (open circle), and 0.1 nm (solid circle). (b) Laser linewidth vs Filter bandwidth at the resonant sweep frequency of 270 Hz.

Fig. 8 (a) Time-varying output center wavelength at the 20-nm sweep and 270-Hz sweep. Solid line is a linearly fitted curve. (b) Deviation of the experimental values from the linear fit curve.

Fig. 9. Peak-hold output spectrum swept over 20 nm by an acoustic frequency sweep over 1 MHz around 68 MHz with a fixed acoustic power.

Fig. 10. Laser output in the time domain (lower trace) when the filter peak is modulated over 20 nm by a saw tooth wave input to the AOTF drive system (upper trace). Significant relaxation oscillation is observed at the beginning of each sweep but dies down within a short fraction of the full sweep.

Fig. 11. (a) The laser output in the time domain at a 9.3-kHz sweep rate (lower trace). The upper trace is a modulation signal applied for the acoustic frequency sweep, (b) max-hold spectrum

Fig. 12. Triangular (solid line) and Square (dotted line) modulated output spectra obtained by synchronous modulations of the filter transmission and peak wavelength.

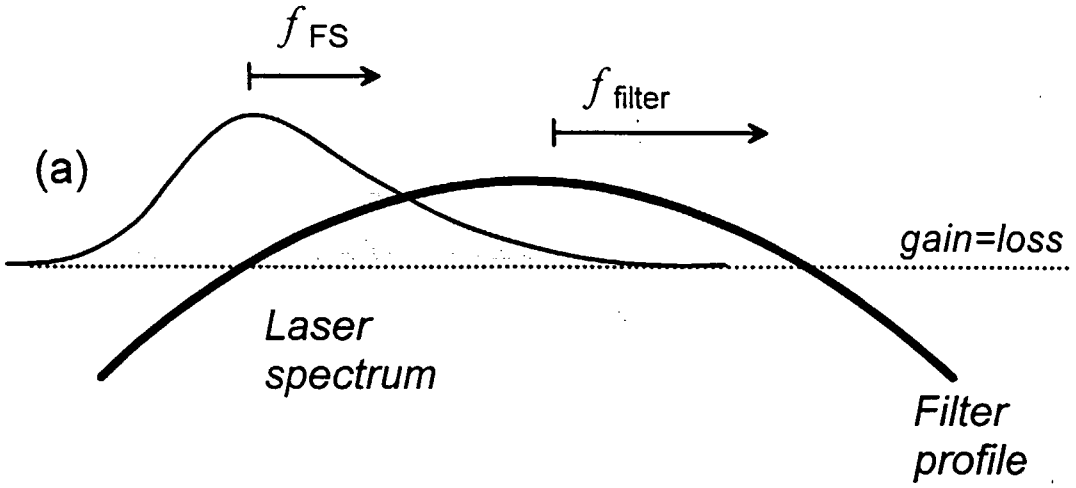
f_{FS}
f_{filter}
(a)
gain=loss
Laser spectrum
Filter profile

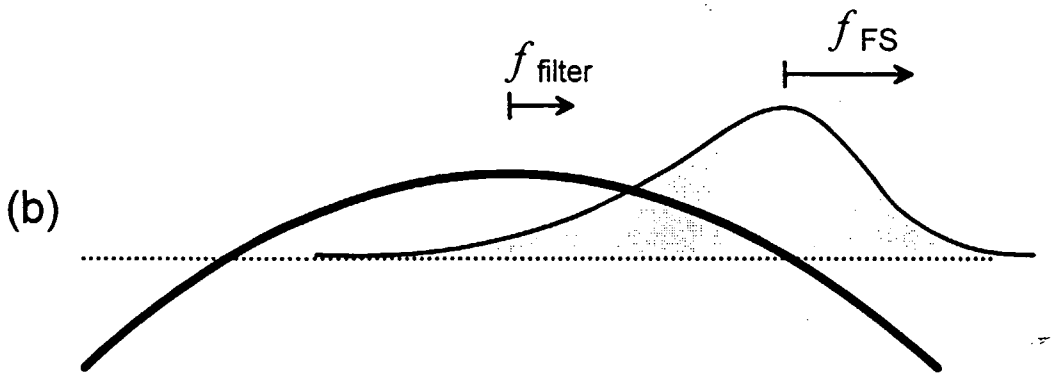
f_{filter}
f_{FS}
(b)

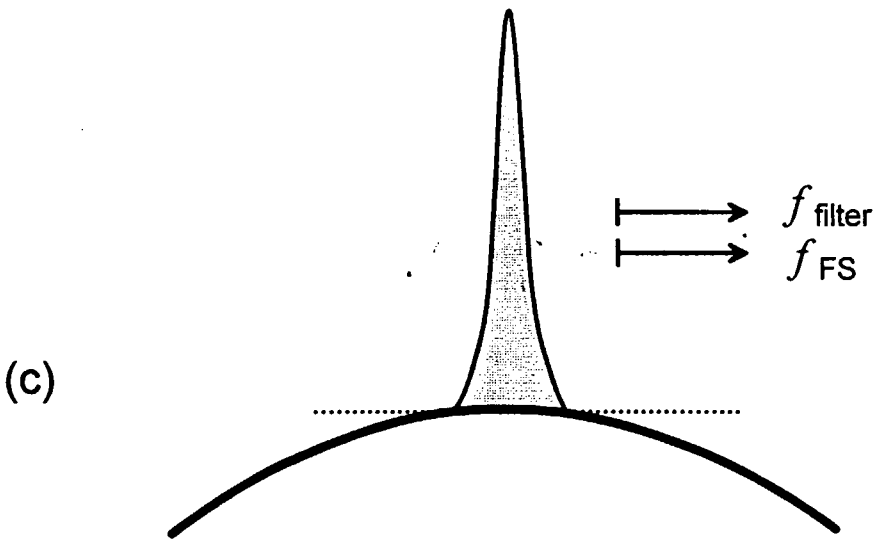
f_{filter}
f_{FS}
(c)

Fig. 1

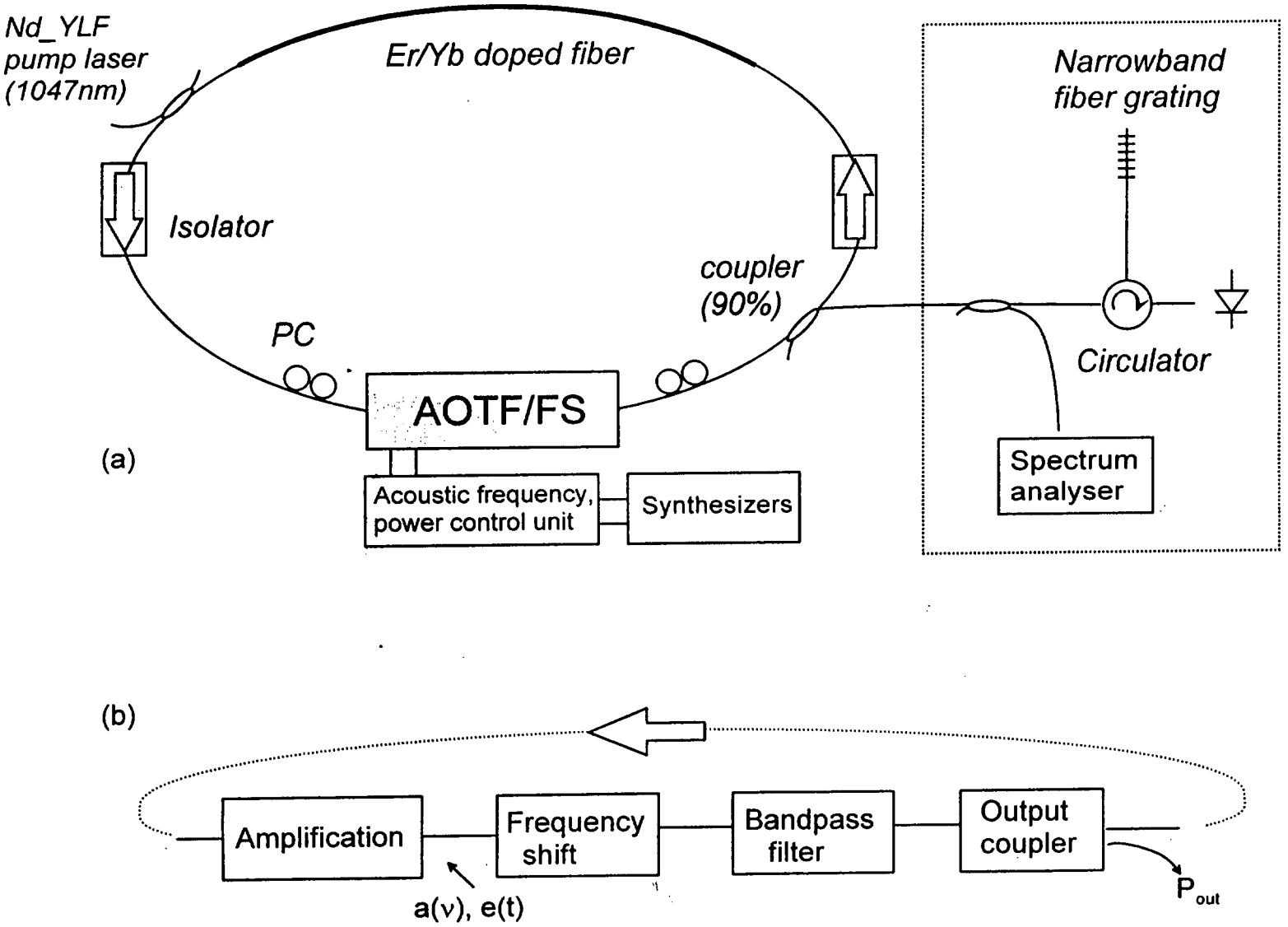
Nd_YLF
pump laser
(1047nm)
Er/Yb doped fiber
Narrowband
fiber grating
Isolator
coupler
(90%)
PC
AOTF/FS
Circulator
(a)
Acoustic frequency,
power control unit
Synthesizers
Spectrum
analyser
(b)
Amplification
Frequency
shift
Bandpass
filter
Output
coupler
a(ν), e(t)
P out

Fig 2

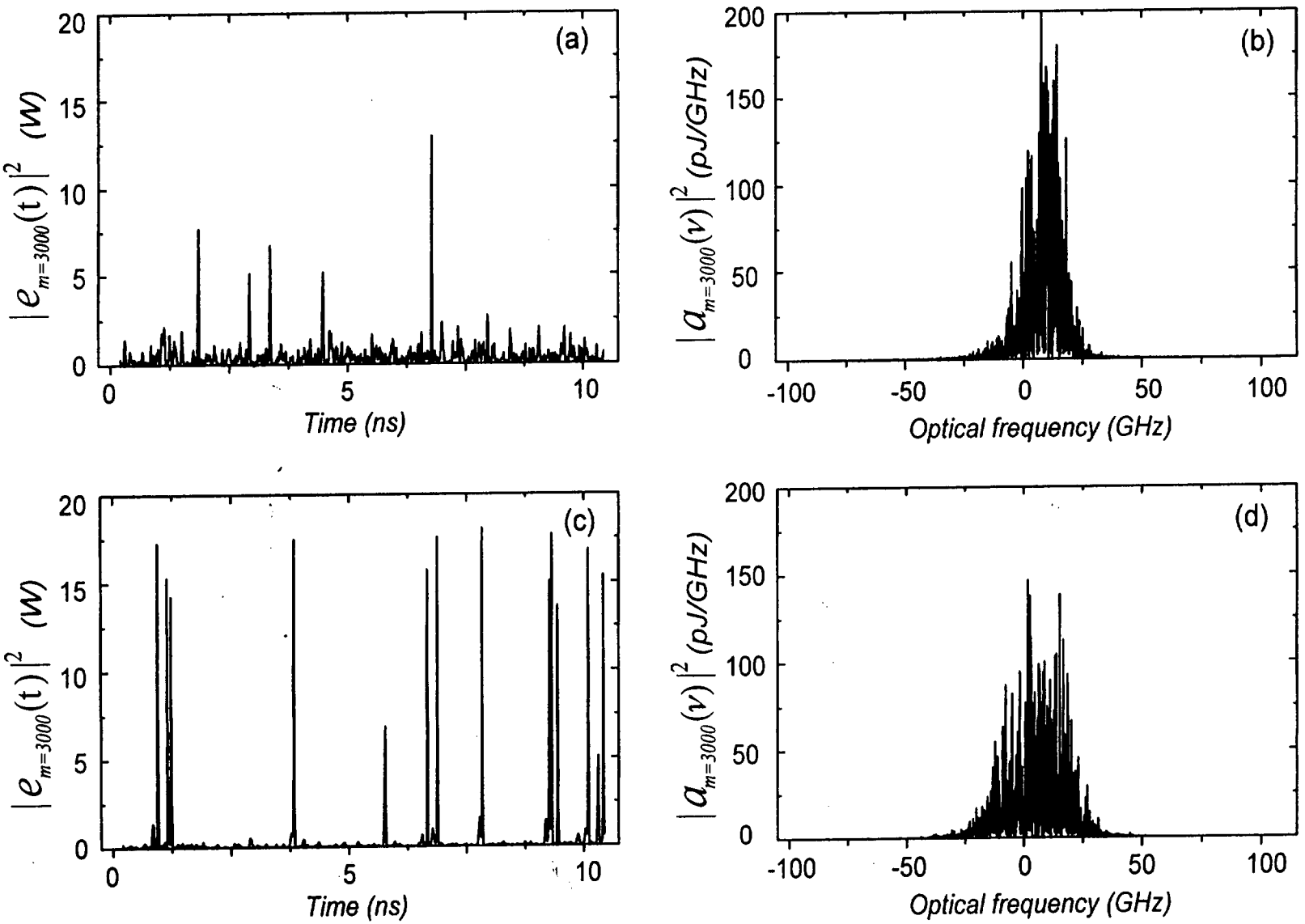
(a)
$|e_{m=3000}(t)|^2$ (W)
Time (ns)
(b)
$|a_{m=3000}(\nu)|^2$ (pJ/GHz)
Optical frequency (GHz)
(c)
$|e_{m=3000}(t)|^2$ (W)
Time (ns)
(d)
$|a_{m=3000}(\nu)|^2$ (pJ/GHz)
Optical frequency (GHz)

Fig. 3

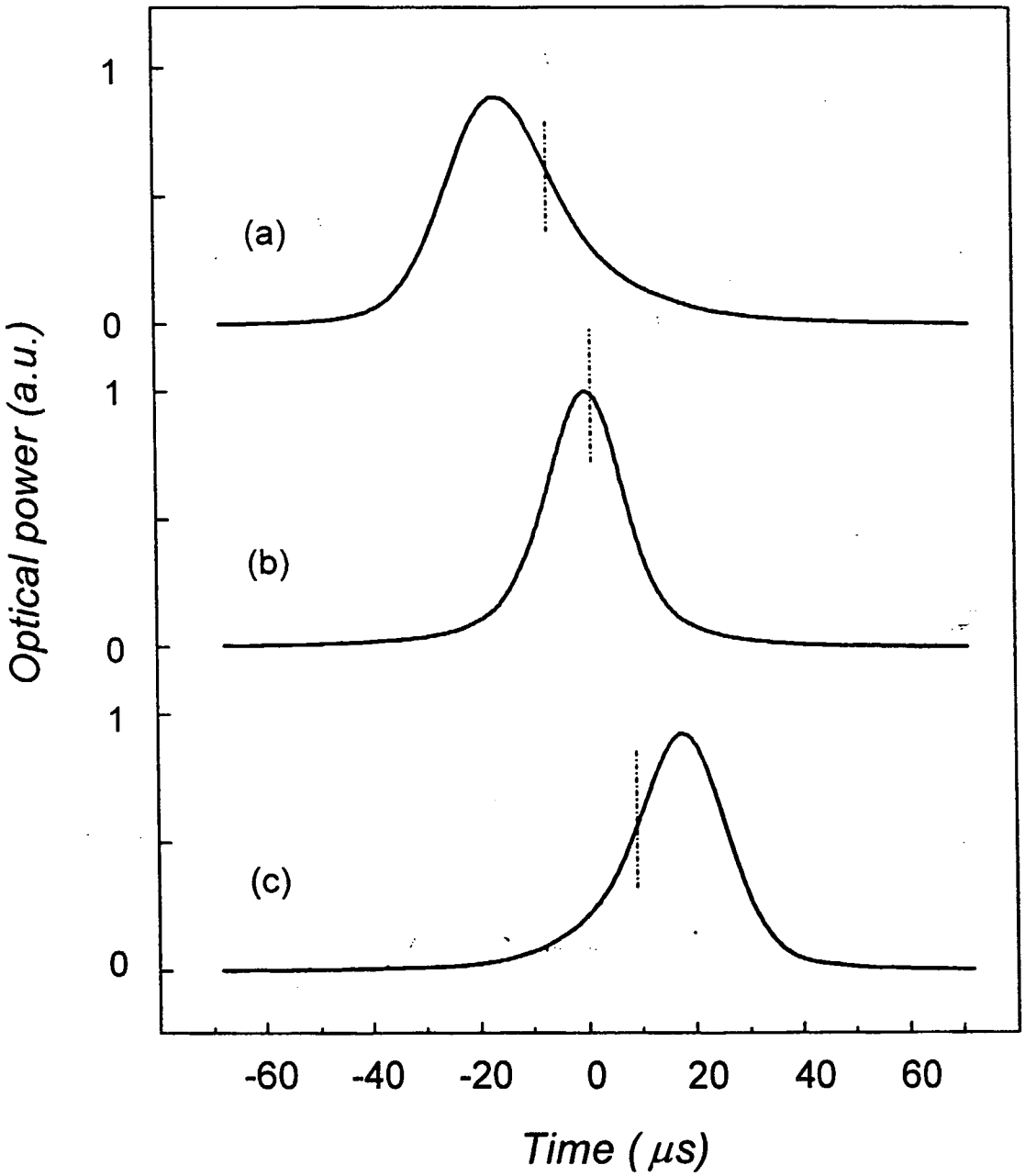

Fig. 4

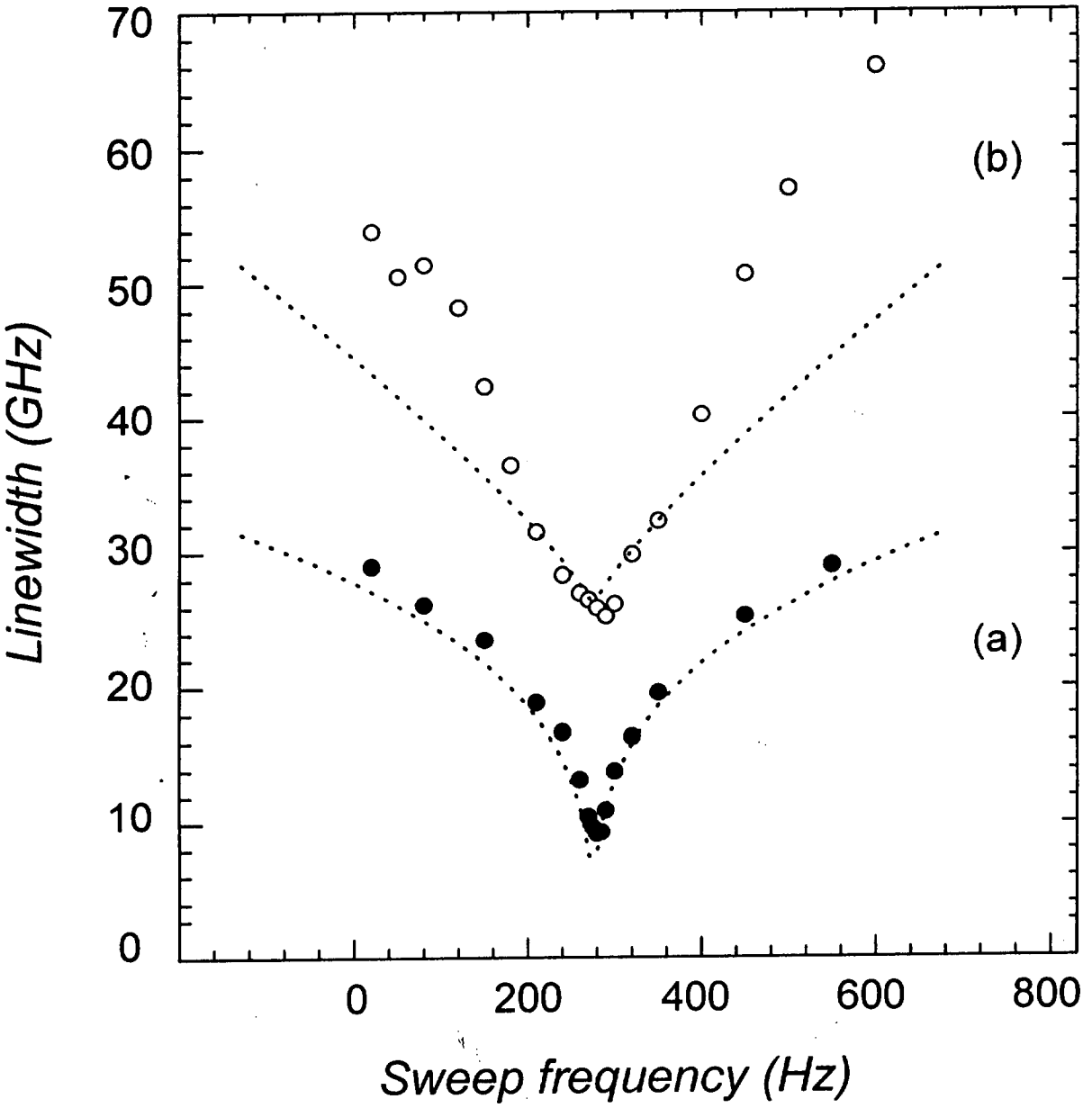
70
60
50
40
30
20
10
0
Linewidth (GHz)
(b)
(a)
0
200
400
600
800
Sweep frequency (Hz)

Fig. 5

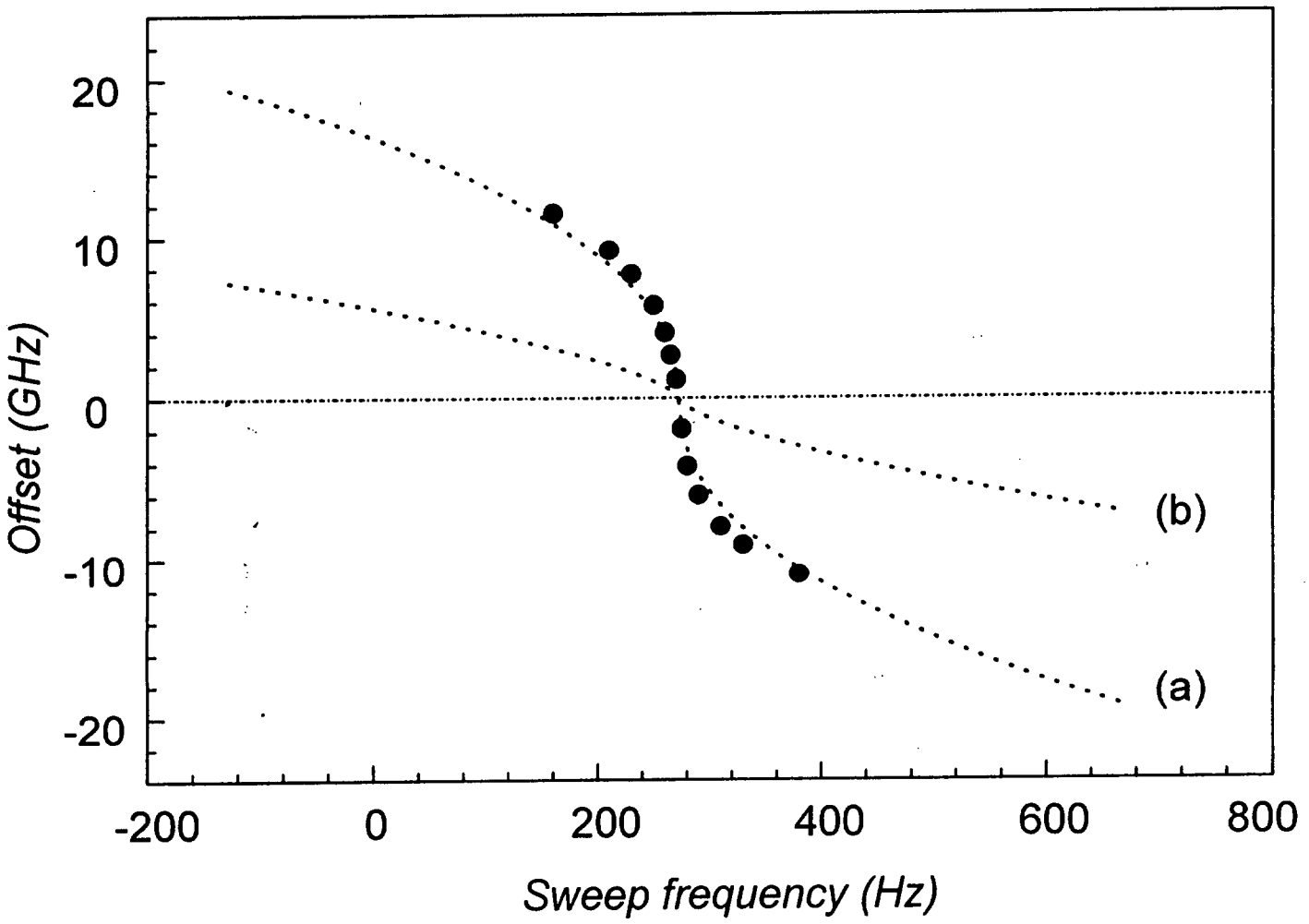
20
10
0
-10
-20
Offset (GHz)
-200
0
200
400
600
800
Sweep frequency (Hz)
(b)
(a)

Fig. 6

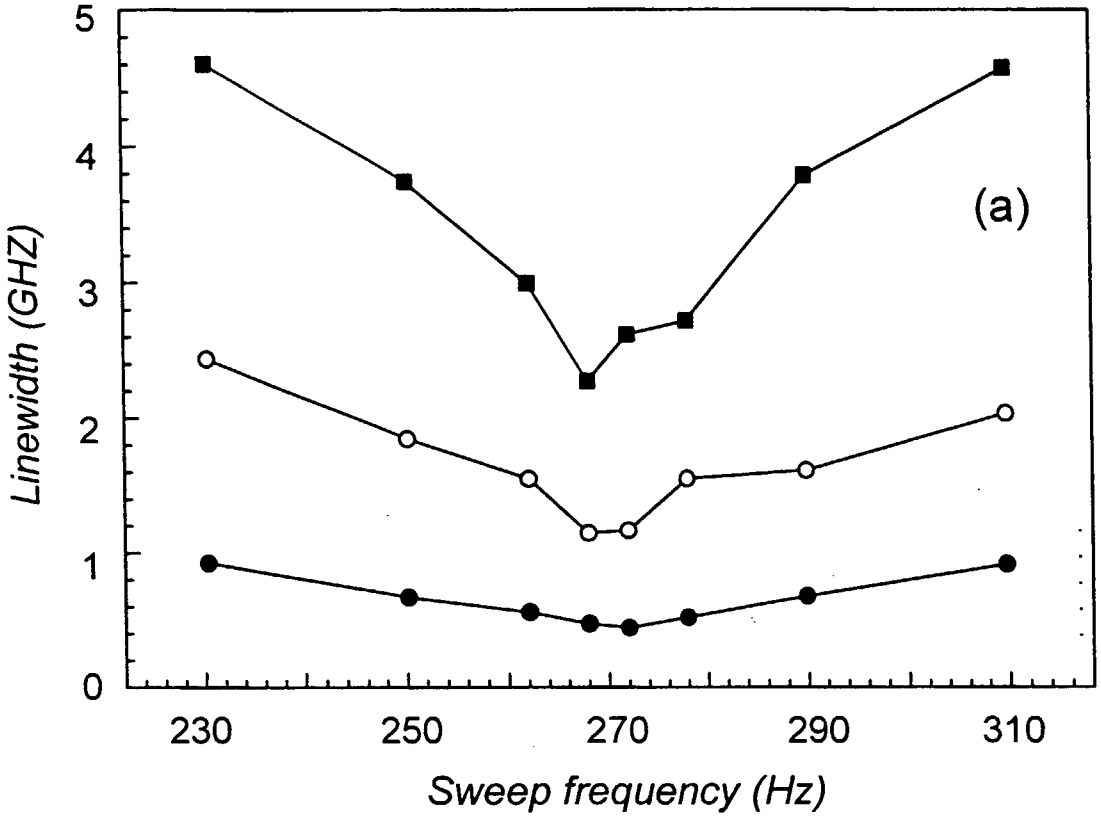
Linewidth (GHZ)
5
4
3
2
1
0
(a)
230
250
270
290
310
Sweep frequency (Hz)

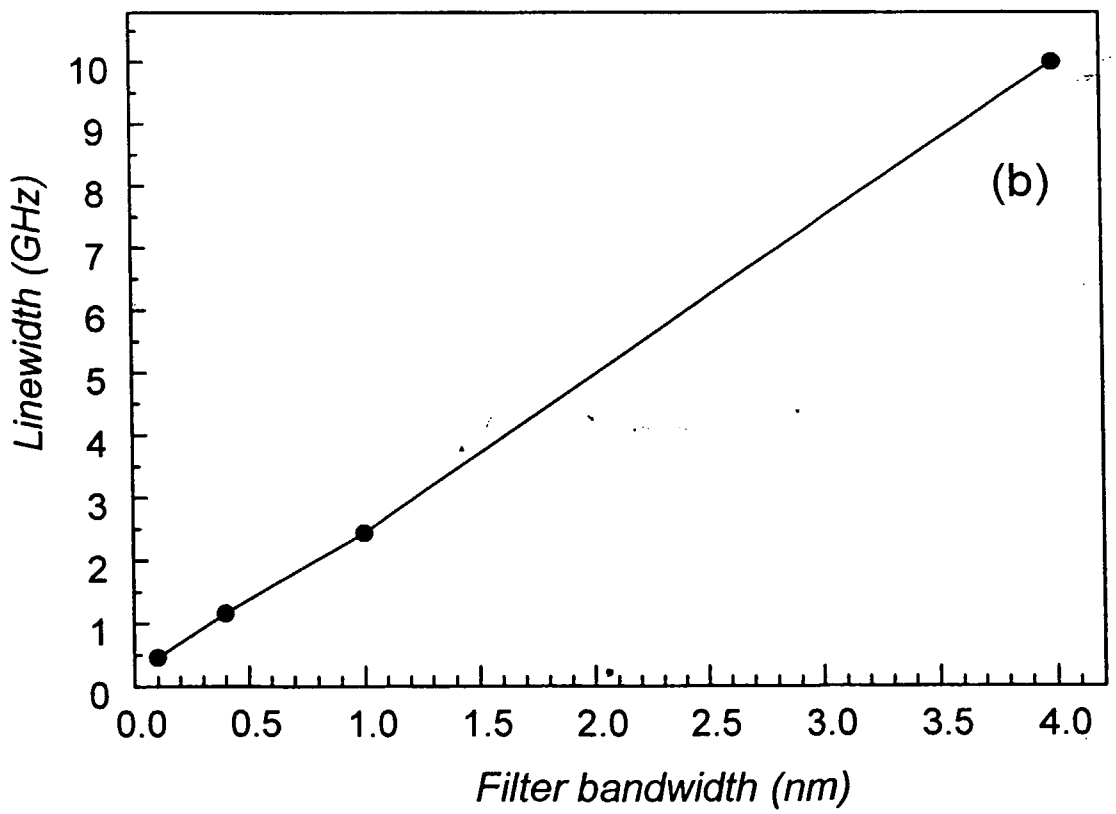
Linewidth (GHz)
10
9
8
7
6
5
4
3
2
1
0
(b)
0.0
0.5
1.0
1.5
2.0
2.5
3.0
3.5
4.0
Filter bandwidth (nm)

Fig. 7

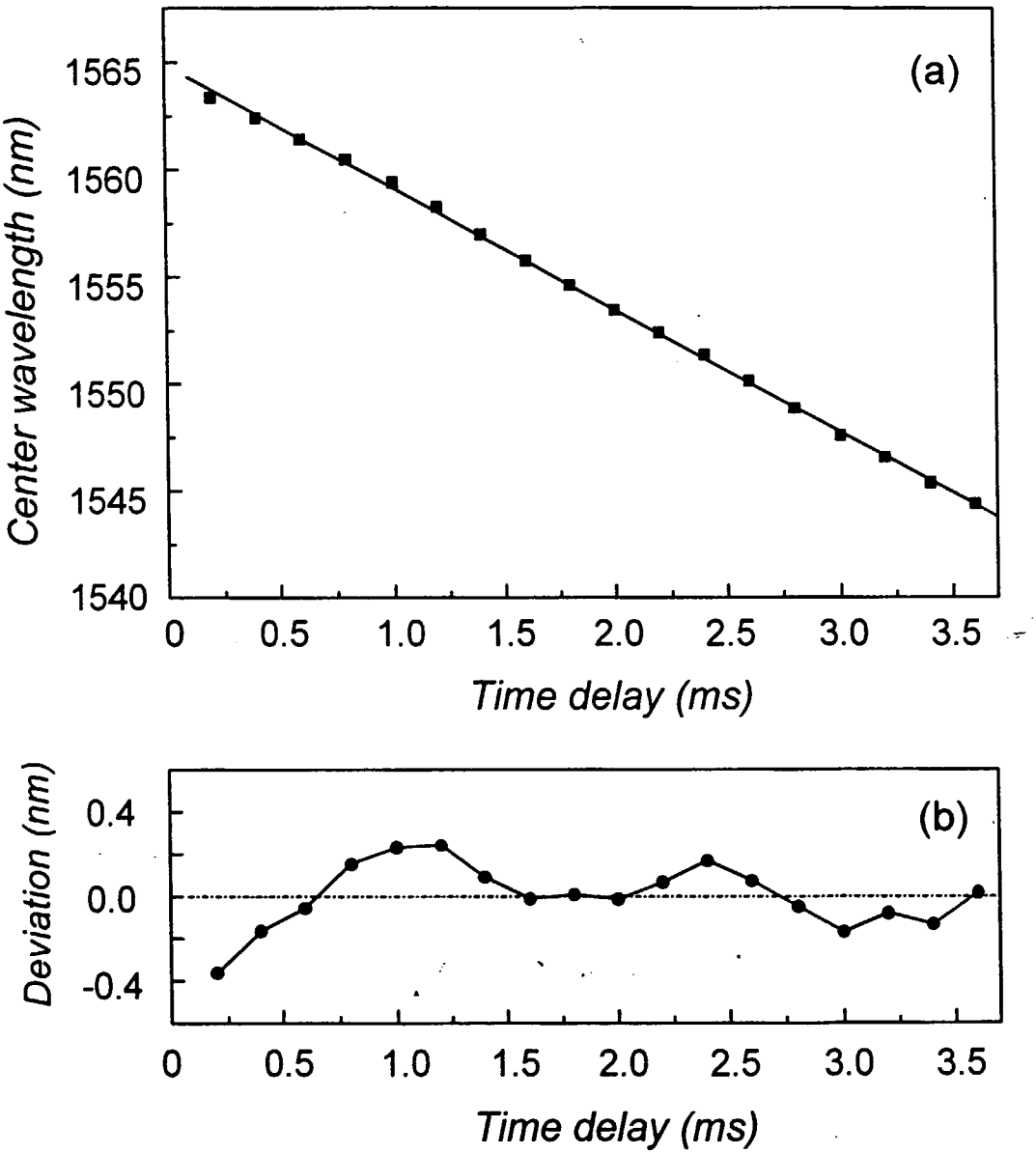
(a)
Center wavelength (nm)
1565
1560
1555
1550
1545
1540
0
0.5
1.0
1.5
2.0
2.5
3.0
3.5
Time delay (ms)
(b)
Deviation (nm)
0.4
0.0
-0.4
0
0.5
1.0
1.5
2.0
2.5
3.0
3.5
Time delay (ms)

Fig. 8

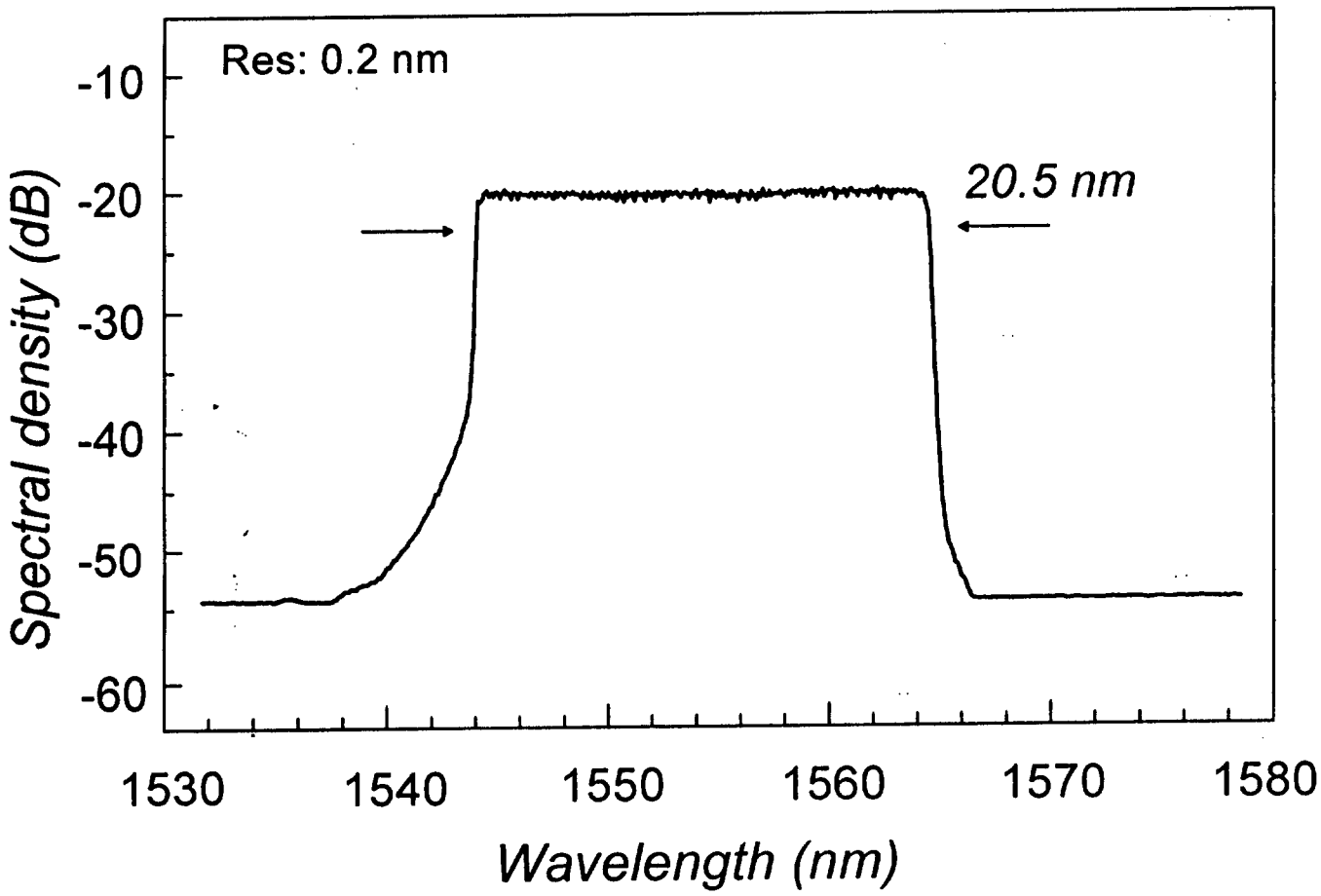
Res: 0.2 nm
20.5 nm
Spectral density (dB)
-10
-20
-30
-40
-50
-60
1530
1540
1550
1560
1570
1580
Wavelength (nm)

Fig. 9

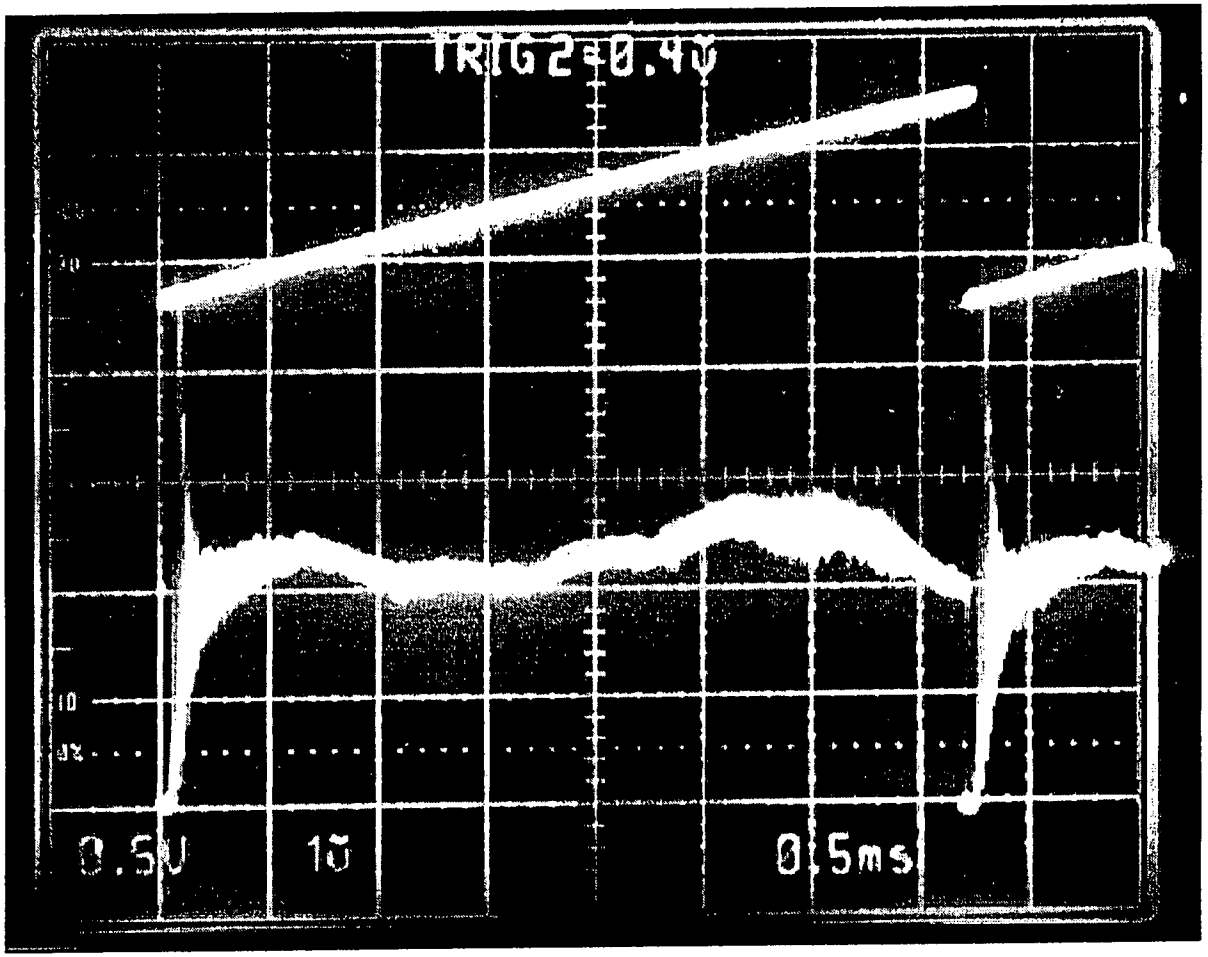

Fig. 10

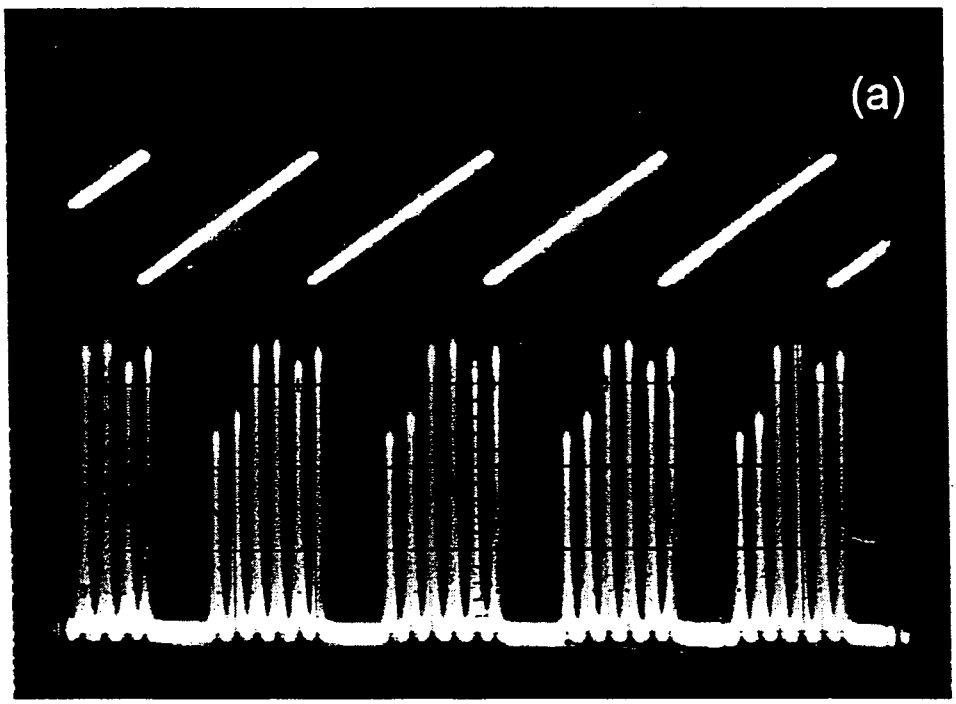

50 μs / div.

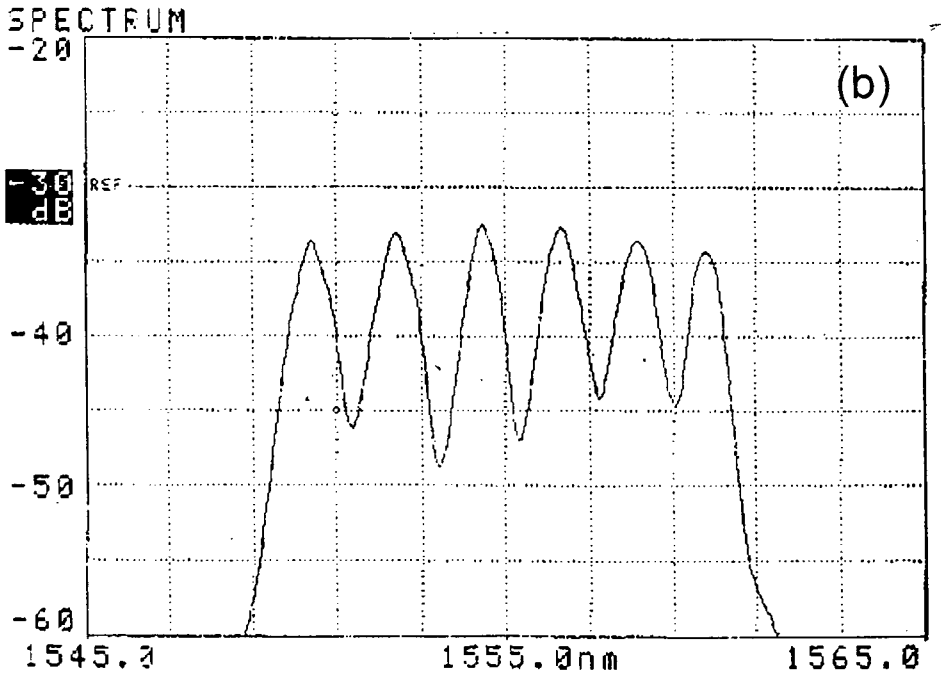

Fig. 11

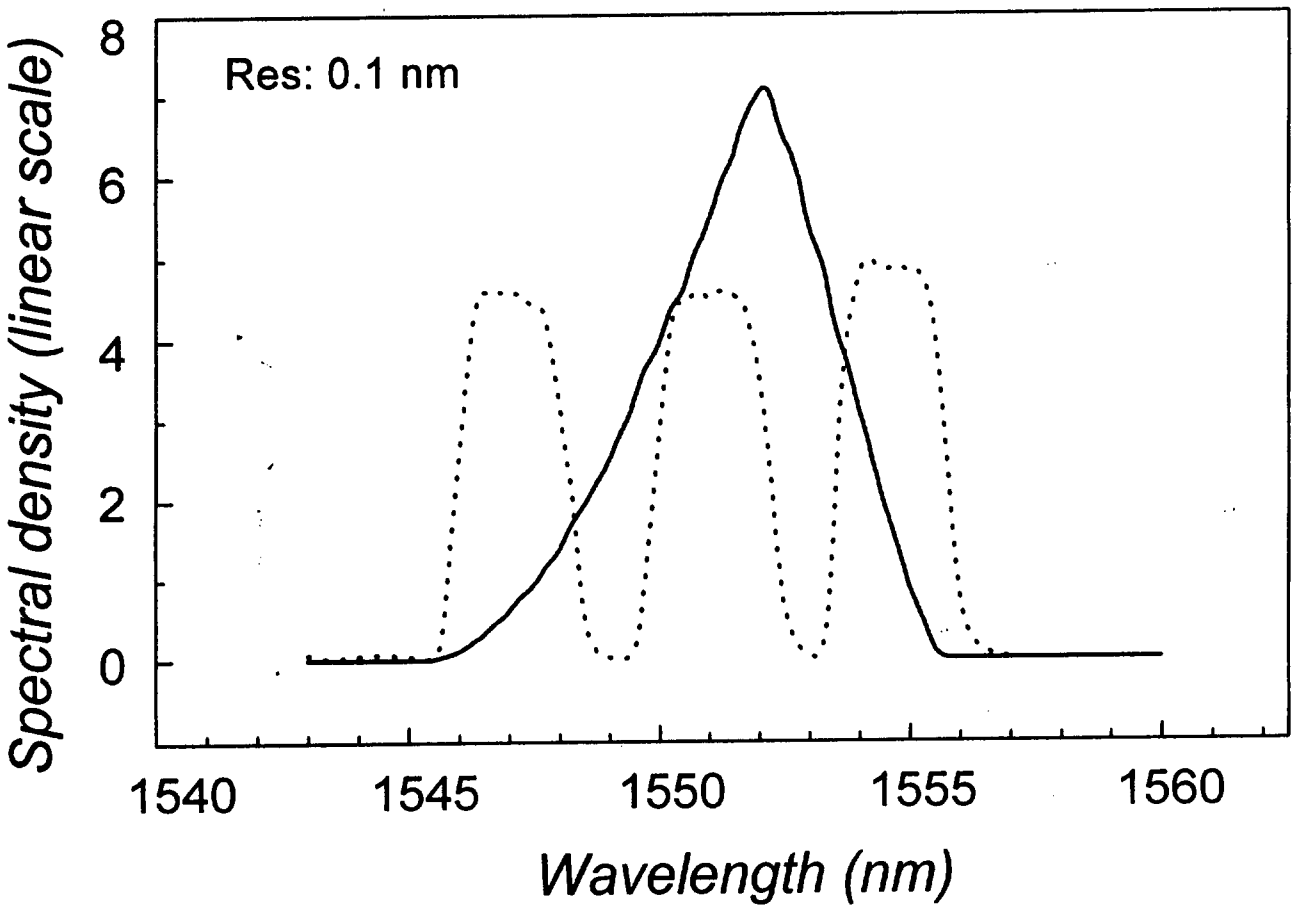
Res: 0.1 nm
Spectral density (linear scale)
8
6
4
2
0
1540
1545
1550
1555
1560
Wavelength (nm)

Fig 12